Energy Recycling Versus Lifetime Quenching in Erbium-Doped 3-μm Fiber Lasers

Markus Pollnau and Stuart D. Jackson

***Abstract*—Based on recently published spectroscopic measurements of the relevant energy-transfer parameters, we performed a detailed analysis of the population mechanisms and the characteristics of the output from Er^{3+}-singly-doped and Er^{3+}, Pr^{3+}-codoped ZBLAN fiber lasers operating at 3 μm, for various Er^{3+} concentrations and pump powers. Whereas both approaches resulted in similar laser performance at Er^{3+} concentrations <4 mol.% and pump powers <10 W absorbed, it is theoretically shown here that the Er^{3+}-singly-doped system will be advantageous for higher Er^{3+} concentrations and pump powers. In this case, energy recycling by energy-transfer upconversion from the lower to the upper laser level can increase the slope efficiency to values greater than the Stokes efficiency, as is associated with a number of Er^{3+}-doped crystal lasers. Output powers at 3 μm on the order of 10 W are predicted.**

***Index Terms*—Diode pumped lasers, infrared lasers, laser biomedical applications, optical fiber lasers, rare earth lasers.**

I. Introduction

Er^{3+}-ACTIVATED lasers in the 3-μm wavelength region have become an important tool in medical applications [1]–[4]. Whereas flashlamp-pumped bulk crystalline laser systems operating at wavelengths near 3 μm have been available for a number of years, diode-pumped CW systems have only recently reached output-power levels that are of interest in microsurgery. Similar output powers of 1.7 W in ZBLAN [5] and 1.8 W in $LiYF_4$ [6] have been reported.

Several methods [7] proved successful to overcome the bottle-neck of this laser under CW pumping as a result of the long $^4I_{13/2}$ lower level lifetime (Fig. 1). First, excited-state absorption (ESA) of pump light from the lower laser level at 800 nm [8], [9] is only efficient in low-doped, core-pumped fiber lasers [10], [11] and cannot be exploited when pumping with low-brightness diode lasers. Second, lifetime quenching by energy transfer (ET) to a Pr^{3+} codopant [12], [13] is successful also under diode pumping [14], [5], [15] but can at best convert each pump photon into one laser photon, leading to slope efficiencies below the Stokes limit [7]. Third, energy-transfer upconversion (ETU) between neighboring active ions in the lower laser level can recycle energy from the lower to the upper laser level [16], [33], thereby increasing the laser slope efficiency by a factor of two to values much greater than the Stokes limit [17], [7]. This regime was successfully demonstrated in bulk crystalline lasers [16], [33], [13], [18]–[20]. However, it has not led to significant improvement of the slope efficiency and output power of 3-μm fiber lasers [21], [22], [7]. It has remained an open question as to what Er^{3+} concentrations and pump powers are necessary so that energy recycling can be exploited successfully in the case of fiber lasers.

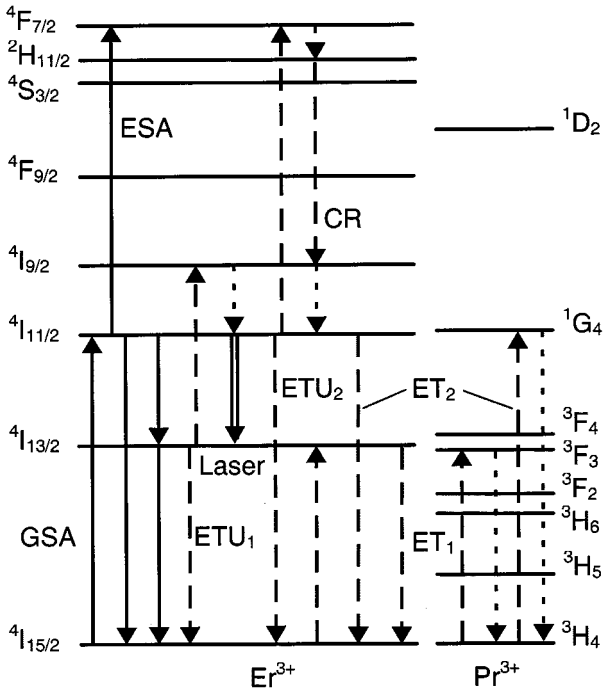

Fig. 1. Partial energy-level scheme of erbium indicating the processes relevant to the energy-recycling and lifetime-quenching regimes of the Er^{3+} 3-μm fiber laser: Direct pumping of the $^4I_{11/2}$ upper laser level by GSA, pump ESA from this level, 3-μm laser transition to the $^4I_{13/2}$ lower laser level, energy-transfer processes such as ETU from the $^4I_{11/2}$ upper and $^4I_{13/2}$ lower laser levels, ET from these levels to the Pr^{3+} codopant, CR from the thermally coupled $^4S_{3/2}$ and $^2H_{11/2}$ levels, as well as subsequent multiphonon relaxations.

It is generally recognized that thermal and thermo-optical issues set limitations to the power scalability of end-pumped bulk laser systems [23]–[25]. Owing to the unfavorable temperature dependence of thermal and thermo-optical parameters [26], the large heat load in the crystal leads, firstly, to a significant temperature increase within the rod, secondly, to strong thermal lensing with pronounced spherical aberrations and, ultimately, to rod fracture in a high-power end-pumped system. These effects are especially pronounced in highly erbium-doped crystals, as the multiphonon relaxations following the efficient

Manuscript received May 15, 2001; revised November 1, 2001. The work of M. Pollnau was supported by the Swiss National Science Foundation. The work of S. D. Jackson was supported by the Australian Research Council.

M. Pollnau is with the Institute of Applied Optics, Department of Microtechnique, Swiss Federal Institute of Technology, CH-1015 Lausanne, Switzerland (e-mail: markus.pollnau@epfl.ch).

S. D. Jackson is with the Optical Fiber Technology Centre, Australian Photonics CRC, the University of Sydney, Australian Technology Park, Eveleigh NSW 1430, Australia.

Publisher Item Identifier S 0018-9197(02)00618-8.

ETU processes (Fig. 1) lead to significant extra heat generation compared to, e.g., 1-μm Nd^{3+} lasers under similar pump conditions [27]. Consequently, the slab geometry was used to reduce the thermal and thermo-optical effects and, hence, to raise the output power from 3-μm $LiYF_4:Er^{3+}$ bulk laser systems [6]. Due to its geometry, the optical fiber provides large flexibility and potentially higher pump and output powers than the bulk system without the drawbacks of thermal and thermo-optical effects. Therefore, the Er^{3+}-doped ZBLAN fiber represents a promising alternative for the construction of a compact and efficient all-solid-state laser emitting at 3 μm.

In this paper, we investigate theoretically the potential to demonstrate significantly higher slope efficiencies and output powers compared to previous demonstrations of 3-μm emission from diode-pumped Er^{3+}-doped ZBLAN double-clad fiber lasers. Based on our recent spectroscopic measurements [28] of the energy-transfer parameters relevant to Er^{3+}-singly-doped and Er^{3+}, Pr^{3+}-codoped ZBLAN bulk glasses, we compare the successfully demonstrated lifetime-quenching regime [5] and the potential energy-recycling regime [7] with respect to slope efficiency and output power. A new fiber design that exploits the energy-recycling regime and takes account of the somewhat low damage thresholds of the mirror coatings at 3 μm and of the ZBLAN fiber itself can be capable of delivering output powers at 3 μm on the order of 10 W, with slope efficiencies in excess of the Stokes limit of 35% under 980-nm pumping.

II. Rate-Equation Model

In a computer simulation considering the relevant energy levels of Er^{3+} (Fig. 1) and processes such as pump ground-state absorption (GSA) and pump ESA from the upper laser level at 980 nm, ground-state bleaching, all lifetimes and branching ratios, ETU and cross relaxation (CR), ET to the Pr^{3+} codopant, stimulated emission at 2.7 μm, and the data relevant to the fiber and resonator, the space-dependent rate equations describing the erbium ZBLAN system were solved numerically. From the calculated population mechanisms, the input–output characteristics of the laser were derived. The population mechanisms for the Er^{3+}-singly-doped and Er^{3+}, Pr^{3+}-codoped ZBLAN systems were considered in the following way.

For the simulation, cylindrical and radially uniform profiles of the pump and the laser modes were assumed. This approximation seems justified because first, the cladding area is large compared to the core area, i.e., the excitation profile is relatively homogeneous over the doped region, and second, the signal mode significantly extends into the cladding (because of the low core/cladding NA chosen discussed below). Consequently, the signal beam extracts the gain almost completely. Let z be the variable representing the discrete longitudinal elements 1 to n covering the fiber length ℓ. The pump radiation from a diode laser operating in the wavelength range 975–985 nm is absorbed via the GSA transition $^4I_{15/2} \rightarrow {}^4I_{11/2}$, as well as the ESA transition $^4I_{11/2} \rightarrow {}^4F_{7/2}$ [29]. The pump power, as well as the cross-sections σ_{GSA} and σ_{ESA}, vary over the wavelength range of the pump emission. In order to investigate the possible influence of ESA at different wavelengths, we consider the diode-laser pump light to be emitted at three different pump wavelengths λ_P over a relatively large wavelength range, with a profile that is centered at the medium wavelength. The values relating to the pump discretization are provided in Table I. At each pump wavelength p, the local absorption coefficient $\alpha(z, p)$ within the longitudinal spatial element z of width $\Delta\ell(z)$ is given by

TABLE I
Pump and Fiber Parameters [Cross-Sections in (10^{-21} cm^2)]

Parameter	Value		
Launch Efficiency η_{in}	70%		
Pump Cladding Area A_{clad}	150 μm × 200 μm		
Inner/Outer Cladding NA	0.5		
Core Radius r_{core}	20 μm		
Core/Inner Cladding NA	0.12		
Pr^{3+} Concentration N_{Pr}	0-0.4×10^{20} cm^{-3} (0-0.25 mol%)		
Pump Wavelength λ_P	975 nm	980 nm	985 nm
Incident Pump Power P	10 W	25 W	10 W
GSA Cross Section σ_{GSA} [29]	2.1	1.7	0.9
ESA Cross Section σ_{ESA} [29]	1.1	0.5	0.2

$$\alpha(z, p) = \sigma_{\mathrm{GSA}}(p)N_0(z) + \sigma_{\mathrm{ESA}}(p)N_2(z). \tag{1}$$

In (1), $N_i(z)$ are the local population densities. The nonaxial symmetry of the rectangular cladding geometry allows for an effective absorption coefficient of the whole fiber to be given by

$$\alpha_{\mathrm{eff}}(z, p) = \alpha(z, p)\pi r_{\mathrm{core}}^2/A_{\mathrm{clad}}. \tag{2}$$

In (2), r_{core} and A_{clad} are the core radius and cladding area, respectively. The powers $P_{\mathrm{in}}(z, p)$ launched into an individual longitudinal element z are calculated from

$$P_{\mathrm{in}}(z, p) = \eta_{\mathrm{in}}P(p)\prod_{z'=1}^{z-1}\{\exp[-\Delta\ell(z')\alpha_{\mathrm{eff}}(z', p)]\} \tag{3}$$

where $P(p)$ are the incident pump powers and η_{in} is the launch efficiency. With (1)–(3), the equations for the local GSA and ESA pump rates $R_{\mathrm{GSA/ESA}}(z)$ summed over the pump wavelengths p read

$$\begin{aligned} R_{\mathrm{GSA/ESA}}(z) = {} & \Sigma_{p=1\cdots3}[\sigma_{\mathrm{GSA/ESA}}(p)N_{0/2}(z)/\alpha(z, p)] \\ & \cdot\{1 - \exp[-\Delta\ell(z)\alpha_{\mathrm{eff}}(z, p)]\} \\ & \cdot\{\lambda_P/(hc\ell\pi r_{\mathrm{core}}^2)P_{\mathrm{in}}(z, p)\}. \end{aligned} \tag{4}$$

where h and c denote Planck's constant and the vacuum speed of light, respectively. Equation (4) considers ground-state bleaching and the population of the ESA level dynamically.

The relevant Er^{3+}:ZBLAN lifetimes τ_i of Table II represent the intrinsic lifetimes of the system at low dopant con-

TABLE II
SPECTROSCOPIC PARAMETERS [28], [14]: RELEVANT LIFETIMES (ms) AND BRANCHING RATIOS (THE OTHER LIFETIMES AND BRANCHING RATIOS HAVE NO SIGNIFICANT INFLUENCE ON THE CALCULATED RESULTS)

Parameter	Value(s)
$^4I_{13/2}$ Intrinsic Lifetime τ_1	9.0
$^4I_{11/2}$ Intrinsic Lifetime τ_2	6.9
$^4F_{9/2}$ Intrinsic Lifetime τ_4	0.12
$^4S_{3/2}$ Intrinsic Lifetime τ_5	0.58
Branching ratios	
$^4I_{11/2} \rightarrow {}^4I_{13/2}\ \beta_{21}, \rightarrow {}^4I_{15/2}\ \beta_{20}$	0.37, 0.63
$^4I_{9/2} \rightarrow {}^4I_{11/2}\ \beta_{32}$	0.99
$^4F_{9/2} \rightarrow {}^4I_{9/2}\ \beta_{43}, \rightarrow {}^4I_{15/2}\ \beta_{40}$	0.85, 0.14
$^4S_{3/2} \rightarrow {}^4F_{9/2}\ \beta_{54}, \rightarrow {}^4I_{13/2}\ \beta_{51}, \rightarrow {}^4I_{15/2}\ \beta_{50}$	0.34, 0.18, 0.44
$^4F_{7/2} \rightarrow {}^4S_{3/2}\ \beta_{65}$	0.99

TABLE III
PARAMETERS OF THE LASER TRANSITION [5], [12], [14]

Parameter	Value
Reflectivity of Fiber Cavity R'	0.04
Losses per Fiber Length κ	23 km^{-1} (= 100 dB/km)
Losses at HR Mirror L'	2%
Boltzmann Factor of Upper Stark Level b_2	0.200
Boltzmann Factor of Lower Stark Level b_1	0.113
Laser Wavelength λ_L	2.71 μm
Stimulated-emission Cross Section σ_{SE}	5.7×10^{-21} cm^2

centration and include radiative as well as multiphonon relaxation. The $^4S_{3/2}$ and $^2H_{11/2}$ levels are thermally coupled and are treated as a combined level. Thermal redistribution within each multiplet is assumed to take place instantaneously. The relevant branching ratios β_{ij} for decay from level i into lower lying levels j are given in Table II. For consistency with former calculations [14], let the Stark transition of the 2.7-μm laser originate from the second Stark level of the $^4I_{11/2}$ multiplet and terminate in the fourth Stark level of the $^4I_{13/2}$ multiplet. Since the Stark-level energies of Er^{3+} are inhomogeneously broadened in ZBLAN and cannot be measured, the Boltzmann factors b_i of upper and lower Stark laser levels (Table III) are taken from $LiYF_4$ [14]. The Stark levels in Er^{3+} are Kramers' degenerate, i.e., the degeneracies are $g_i = 2$. The influence of ETU and ET from the $^4I_{13/2}$ and $^4I_{11/2}$ levels, as well as CR from the

TABLE IV
SPECTROSCOPIC PARAMETERS [28]: Er^{3+} CONCENTRATIONS (mol.% AND 10^{20} cm^{-3}), FIBER LENGTHS (m), AND ENERGY-TRANSFER PARAMETERS (10^{-17} cm^3s^{-1}). THE PARAMETERS FOR ET $Er^{3+} \rightarrow Pr^{3+}$ ARE GIVEN FOR A Pr^{3+} CONCENTRATION OF 0.4×10^{20} cm^{-3}

Parameter	Value(s)		
Er^{3+} concentration (mol.%)	1.25	5.00	8.75
Er^{3+} concentration (10^{20} cm^{-3})	2	8	14
Fiber Length ℓ	2.00	0.50	0.29
Optical Fiber Length ℓ_{opt}	3.00	0.75	0.43
ETU Parameter from $^4I_{13/2}$ W_{11}	1.30	2.80	6.70
ETU Parameter from $^4I_{11/2}$ W_{22}	0.20	1.00	1.90
CR Parameter from $^4S_{3/2}$ / $^2H_{11/2}$ W_{50}	0.60	2.40	3.30
ET Parameter from $^4I_{13/2}$ W_1	2.10	9.00	16.8
ET Parameter from $^4I_{11/2}$ W_2	0.15	0.90	2.10

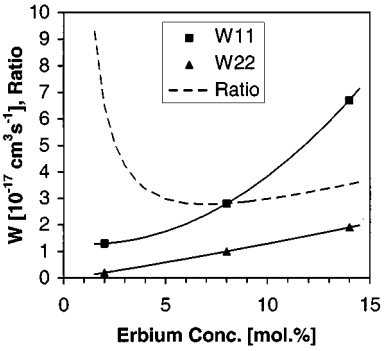

Fig. 2. Measured [13] ETU parameters W_{11} (squares) and W_{22} (triangles) from the $^4I_{13/2}$ lower and $^4I_{11/2}$ upper laser levels, respectively, polynomial fits (solid lines), and ratio W_{11}/W_{22} (dashed line).

$^4S_{3/2}/^2H_{11/2}$ levels is investigated in the simulation using the macroscopic transfer parameters (Table IV) measured in [28]. For the other Er^{3+} concentrations investigated in the simulation, the transfer parameters were interpolated by polynomial fits (for example, see the solid lines for the values of the ETU parameters in Fig. 2). W_{11} is the parameter for the ETU process ($^4I_{13/2}$, $^4I_{13/2}$) $\rightarrow$ ($^4I_{9/2}$, $^4I_{15/2}$), W_{22} is the parameter for the ETU process ($^4I_{11/2}$, $^4I_{11/2}$) $\rightarrow$ ($^4F_{7/2}$, $^4I_{15/2}$), W_{50} is the parameter for the CR process ($^4S_{3/2}/^2H_{11/2}$, $^4I_{15/2}$) $\rightarrow$ ($^4I_{9/2}$, $^4I_{13/2}$), W_1 is the parameter for the ET process Er^{3+} $^4I_{13/2}$ $\rightarrow$ Pr^{3+} $^3F_3$, and W_2 is the parameter for the ET process Er^{3+} $^4I_{11/2}$ $\rightarrow$ Pr^{3+} $^1G_4$. Rapid intrinsic relaxation within the Pr^{3+} ions to the ground state is assumed.

With the above considerations, the rate equations for the local population densities $N_i(z)$ read

$$dN_6(z)/dt = R_{ESA}(z) - \tau_6^{-1}N_6(z) + W_{22}N_2^2(z) \quad (5)$$

$$dN_5(z)/dt = \beta_{65}\tau_6^{-1}N_6(z) - \tau_5^{-1}N_5(z) - W_{50}N_5(z)N_0(z) \quad (6)$$

$$dN_4(z)/dt = \Sigma_{i=5\ldots6}[\beta_{i4}\tau_i^{-1}N_i(z)] - \tau_4^{-1}N_4(z) \quad (7)$$

$$dN_3(z)/dt = \Sigma_{i=4\ldots6}[\beta_{i3}\tau_i^{-1}N_i(z)] - \tau_3^{-1}N_3(z) + W_{50}N_5(z)N_0(z) + W_{11}N_1^2(z) \quad (8)$$

$$dN_2(z)/dt = R_{\mathrm{GSA}}(z) - R_{\mathrm{ESA}}(z) + \Sigma_{i=3\ldots6}[\beta_{i2}\tau_i^{-1}N_i(z)] - \tau_2^{-1}N_2(z) - 2W_{22}N_2^2(z) - W_2N_2N_{\mathrm{Pr}} - R_{SE}(z) \quad (9)$$

$$dN_1(z)/dt = \Sigma_{i=2\ldots6}[\beta_{i1}\tau_i^{-1}N_i(z)] - \tau_1^{-1}N_1(z) + W_{50}N_5(z)N_0(z) - 2W_{11}N_1^2(z) - W_1N_1N_{\mathrm{Pr}} + R_{\mathrm{SE}}(z) \quad (10)$$

$$N_{\mathrm{Er}} = \Sigma_{i=0\ldots6}N_i(z). \quad (11)$$

In (9)–(11), N_{Er} and N_{Pr} are the Er^{3+} and Pr^{3+} concentrations, respectively. The rate equation for the photon density ϕ is given by

$$d\phi/dt = (\ell/\ell_{\mathrm{opt}})\sum_{z=1}^{n} R_{\mathrm{SE}}(z) - \{-\ln[R'(1-L')] + 2\kappa\ell\}c\phi/(2\ell_{\mathrm{opt}}) \quad (12)$$

where

- ℓ_{opt} optical fiber length
- R' reflectivity of the output mirror of the fiber cavity
- L' losses at the highly reflective mirror
- κ losses per fiber length.

The stimulated-emission rate $R_{\mathrm{SE}}(z)$ is

$$R_{\mathrm{SE}}(z) = [b_2N_2(z) - (g_2/g_1)b_1N_1(z)]\sigma_{\mathrm{SE}}c\phi. \quad (13)$$

In (13), σ_{SE} is the stimulated-emission cross-section. The output power P_{out} is calculated from

$$P_{\mathrm{out}} = 0.5c\phi(hc/\lambda_L)\pi r_{\mathrm{core}}^2[-\ln(1-R')]. \quad (14)$$

In (14), λ_L is the laser wavelength. The rate equations are solved with a longitudinal discretization of the active medium of $n = 8$ elements of equal length and in a Runge–Kutta calculation of fourth order. This discretization consideres the influence of the nonuniform pump absorption and excitation densities on the nonlinear population mechanisms with sufficient accuracy.

III. Fiber Design

Naturally, the idea is born first and the optimization of the fiber design comes at the end of this procedure. Nevertheless, we start here with the presentation of the guidelines for the fiber design, because the results of the comparison of the two operational regimes that will follow in the next section will be presented only for the set of parameters optimized for efficient pumping, on the one hand, and the damage threshold of the mirror coatings and fiber, on the other hand. The fiber design proposed here does not take into account possible damage owing to pump-induced heat load, because firstly, it is difficult to estimate convective cooling by air in the simulation, and secondly, the thermal conductivities of highly rare-earth-doped fluorozirconate glasses and specific fiber coatings are unknown.

The following issues have to be taken into consideration when an attempt is made to significantly scale the output power at 3 μm from Er^{3+}-doped fiber lasers. First, whereas modified ZBLAN glasses can be doped with rare-earth concentrations of $\sim$20 mol.% [30], the concentrations in commercially available low-loss ZBLAN fibers are currently limited to some 10–12 mol.%. The Er^{3+} concentration determines the values of the energy-transfer parameters [28]. Specifically, the ratio of the ETU parameters W_{11} and W_{22} from the lower and upper laser levels is relevant to the slope efficiency in the energy-recycling regime [17], [7]. From the measured ETU parameters [28] displayed in Fig. 2, we see that this ratio (dashed line) varies significantly with Er^{3+} concentration. To investigate the influence of ETU, we used the Er^{3+} concentration as a free design parameter. We will discuss the changes in the population mechanisms and consequent laser performance in detail in the next section. In the simulation, the fiber length was adjusted accordingly to assure the same absorption of 90% of the launched pump power at low pump power, i.e., without consideration of the influences of ground-state bleaching and ESA, for each Er^{3+} concentration (Table III).

Second, since the laser will be operated many times above threshold, the slope efficiency rather than the pump threshold is the parameter relevant for optimized output power. Consequently, the lifetime of the upper laser level that is quenched in the presence of the Pr^{3+} codopant does not influence the laser performance significantly. Nevertheless, this parameter was taken into account in the simulation.

Third, from our former experiments, we have learned that the output-power limitation relates predominantly to the potential damage of the mirror coatings due to the high (pump or signal) intensity traveling in the active fiber core. In the core-pumped experiments [10], it was frequently the front fiber end that burned away because of the high Ti : sapphire pump intensity focused onto this end of the fiber and the mirror butt-coupled to it. In the cladding-pumped experiments [5], [15], at certain times, the rear fiber end that was butt-coupled to a high-reflectivity mirror started burning owing to the high signal intensity at this fiber end. From both types of experiments, we estimated the damage threshold of the ZnS coatings to be $\sim$1 MW/cm^2. For an anticipated output power of 10 W, this requires a core radius of $\sim$20 μm. This large core radius enforces a very low core/cladding NA if single-mode operation at 3 μm is to be maintained. Since, however, in this case the mode profile of the signal extends significantly into the cladding, higher propagation losses can be expected at the pump-cladding/second-cladding boundary. Alternatively, a slightly higher NA can be used and oscillation of higher order transverse modes can be avoided by appropriate bending of the fiber.

Fourth, the results of our former double-clad experiments [5], [15] have shown that the pump-coupling efficiency of our laser diode was only $\sim$50%. In order to increase this crucial parameter to $\sim$70% or more, we designed the fiber with an increased cladding area (Table I) which, unfortunately, reduces the effective absorption coefficient in (2) and results in increased fiber lengths. However, this effect is over-compensated by increased absorption due to the higher Er^{3+} concentrations available. We also take advantage of the fast development in diode-laser technology, which has led to an increase in brightness of the diode-laser output by a factor of two since our last experiments.

IV. Comparison of Operational Regimes

In this section, the aspects that are of paramount importance when comparing the energy-recycling and lifetime-quenching regimes shall be discussed in detail.

A. Fundamental Differences

In the ideal co-doped system, i.e., when we choose a Pr^{3+} concentration that is large enough to quench the lifetime of the Er^{3+} lower laser level completely, the situation is close to that of the so-called "four-level laser" system, even though the upper laser level is pumped directly in this case. Ions excited in the $^4I_{13/2}$ lower laser level transfer their energy to the co-dopant immediately, and the excited co-dopant returns to its ground state by fast multiphonon relaxation. The lower laser level is completely empty, no matter how strong the pump intensity, and hence, there is no ETU from this level. The excitation density of the $^4I_{11/2}$ upper laser level is clamped to the threshold inversion, i.e., it depends solely on the overall resonator loss. The loss mechanisms in this situation are the ESA, ETU, ET, and intrinsic decay (fluorescence and multiphonon) processes from the upper laser level. The rates of the ET and intrinsic decay processes depend linearly on the excitation density of the upper laser level and decrease its lifetime. These processes are relevant to the threshold pump power only and do not influence the slope efficiency of the laser. Since the excitation density of the upper laser level is low, the ESA and ETU losses are also small. In this situation, almost all the absorbed pump photons contribute to excitation of the upper laser level and most of these excitations lead to the emission of one laser photon each, i.e., each pump photon is converted into one laser photon. If the internal resonator losses are small, the slope efficiency approaches the Stokes limit, defined as the ratio of laser-to-pump photon energies. However, it is impossible to overcome this fundamental limitation in the ideal co-doped situation.

In contrast, in the singly-doped system, the lifetime of the lower laser level is long. The higher the pump intensity, the higher is the population density of this level. This level is depopulated by intrinsic decay and ETU. In the ideal singly-doped system, ETU is the dominating depletion mechanism and all the ions in the lower laser level undergo this process. Half of the ions are upconverted to the upper laser level, thereby contributing to laser emission a second time without the consumption of a second pump photon. In this situation, the slope efficiency surpasses the Stokes limit and approaches a value of twice the Stokes limit [17], [7]. Thus, energy recycling from the lower to the upper laser level in the ideal singly-doped fiber is a significant advantage over lifetime quenching in the ideal co-doped system, as it potentially leads to higher output power. Since, however, the excitation density of the lower laser level increases with pump intensity, the excitation density of the upper laser level that is clamped to the threshold inversion also increases. This higher excitation of the laser levels inevitably results in the same amount of ground-state bleaching and, therefore, reduced pump absorption. In addition, unlike the ideal co-doped system, ETU from the upper laser level can now become a relevant loss mechanism. If ETU from the lower laser level is not efficient and the depletion of this level occurs partly via intrinsic decay, the disadvantages of this particular operational regime can exceed any advantage.

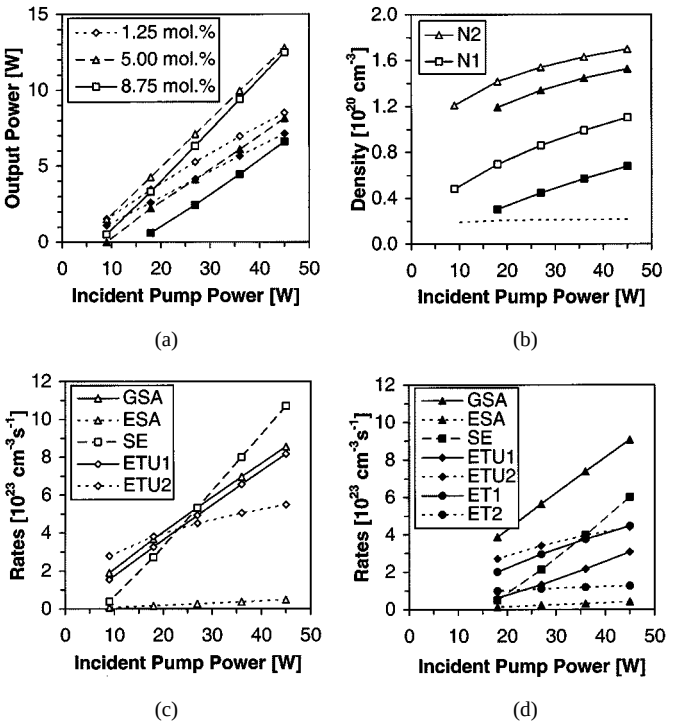

Fig. 3. Calculated performance of 980-nm high-power cladding-pumped ZBLAN : Er^{3+} fiber lasers at 2.7 μm, singly Er^{3+} doped (open symbols) and co-doped with 0.25 mol.% Pr^{3+} (solid symbols), versus incident pump power. (a) Input–output curves for different Er^{3+} concentrations. Data taken at the front end of the fiber for an Er^{3+} concentration of 8.75 mol.%, for pump powers above laser threshold. (b) Population densities N_2 and N_1 of upper and lower laser levels, respectively, and inversion density ΔN (dotted line). Transition rates of the relevant excitation and depletion processes for: (c) singly doped and (d) co-doped fibers. The ETU rates are given for a single ion, i.e., the depletion rates of the laser levels by ETU are twice as large, because two ions are involved in each ETU process.

B. Calculated Results

At the Er^{3+} concentrations of <5 mol.% and pump powers of <10 W absorbed that have been investigated experimentally so far, the slope efficiencies obtained from both operational regimes were found to be similar under 800-nm [5], [22] as well as 980-nm pumping [15], [21]. The population mechanisms at these concentration and power levels were discussed in detail elsewhere [14], [31], [7]. With the considerations of the fiber design discussed in Section III, we performed calculations of the population mechanisms and laser performance by use of the rate equations of Section II for Er^{3+} concentrations of ≥ 5 mol.% and pump powers of >10 W absorbed. The results are presented in Figs. 3 and 4. The specific cases investigated in our simulations are not identical with the ideal cases discussed above; however, they exhibit tendencies toward either of the two extremes.

1) Ground-State Bleaching: We find in the simulation that ground-state bleaching occurs at low Er^{3+} concentration in both, the singly-Er^{3+}-doped and Er^{3+}, Pr^{3+}-codoped fibers, because only a small amount of active ions is available. This bleaching occurs predominantly at the front fiber end and is larger in the ETU regime. Over the whole fiber length,

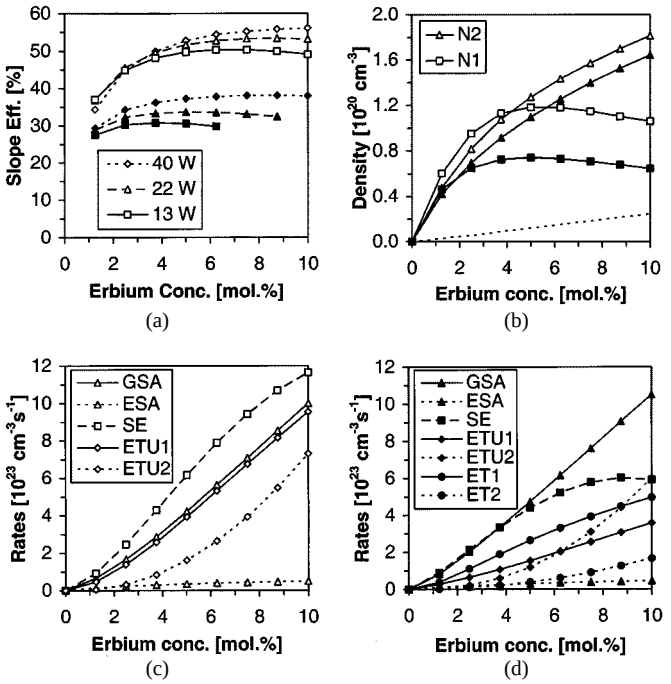

Fig. 4. Calculated performance of 980-nm high-power cladding-pumped ZBLAN : Er^{3+} fiber lasers at 2.7 μm, singly Er^{3+} doped (open symbols), and co-doped with 0.25 mol.% Pr^{3+} (solid symbols), versus Er^{3+} concentration. (a) Slope efficiencies for different incident pump powers. Data taken at the front end of the fiber for the highest incident pump power of 45 W. (b) Population densities N_2 and N_1 of upper and lower laser levels, respectively, and inversion density ΔN (dotted line). Relevant transition rates for: (c) singly-doped and (d) co-doped fibers. The ETU rates are given for a single ion, i.e., the depletion rates of the laser levels by ETU are twice as large, because two ions are involved in each ETU process.

this effect results in a reduction of the fraction of launched pump power absorbed from 90% at low pump power to ~82%–85% at the highest incident pump power of 45 W in the lowest-concentration Er^{3+}-doped fiber. At high Er^{3+} concentration, practically no ground-state bleaching occurs. The relatively small amount of bleaching indicates that both lifetime quenching by ET in the co-doped and depletion by ETU in the singly-doped fibers work well in the situations investigated. As a consequence, the input–output curve exhibits a saturation effect only in the case of the singly Er^{3+}-doped fiber (energy-recycling regime) at low Er^{3+} concentration [open diamonds in Fig. 3(a)] and the ESA rates are generally small compared to the GSA rates. Compare the triangles with the dotted (ESA) and solid lines (GSA) in Figs. 3(c) and (d) and 4(c) and (d). The significant decrease in slope efficiency with decreasing Er^{3+} concentration in the singly-doped system [open symbols in Fig. 4(a), left-hand side] is not a consequence of the slightly decreased fraction of pump power absorbed, but reflects the decreasing efficiency of the energy-recycling process.

2) Output Power and Slope Efficiency: The input–output curves for different Er^{3+} concentrations and slope efficiencies versus the Er^{3+} concentration for different pump powers are shown in Figs. 3(a) and 4(a), respectively. The threshold pump powers [Fig. 3(a)] might be somewhat overestimated due to the uncertainty in the value of the stimulated-emission cross section. The stimulated-emission rates [squares in Fig. 3(c) and (d)] and, thus, the input–output curves, are not linear, leading to an increase of the slope efficiencies with pump power. The reason is that the excitation density N_1 of the lower laser level [squares in Fig. 3(b)] and thus, energy recycling from the lower to the upper laser level by ETU_1 [diamonds with solid lines in Fig. 3(c) and (d)] increase with pump power. Since this process is more efficient in the singly doped system, slope efficiencies can exceed the Stokes limit [open symbols in Fig. 4(a)] and output powers on the order of 10 W can be expected in the energy-recycling regime at higher Er^{3+} concentrations [open symbols in Fig. 3(a)].

3) Threshold Inversion: Dotted lines indicate the inversion density $\Delta N = b_2 N_2 - b_1 N_1$ at the fiber front end versus incident pump power [Fig. 3(b)] and Er^{3+} concentration [Fig. 4(b)]. The inversion density is practically identical for singly- and co-doped fibers. It is kept constant at laser threshold for all pump powers [Fig. 3(b)]. The minimal increase with pump power that is observed at the front fiber end [Fig. 3(b)] is compensated over the whole fiber length. Only in the case of the codoped fiber at 9 W of incident pump power [not shown in Fig. 3(b)], the inversion drops below laser threshold; c.f. the input–output curve (solid squares) in Fig. 3(a). The absorption length decreases inversely proportional to the Er^{3+} concentration, and so does the gain length. As a consequence, the inversion at the front end of the fiber increases proportional to the Er^{3+} concentration [Fig. 4(b)], thus keeping the gain over the whole fiber length at threshold condition.

4) Excitation Densities of the Laser Levels: Figs. 3(b) and 4(b) display the population densities of the laser levels at the front fiber end versus pump power (for 8.75 mol.% Er^{3+}-doped fibers) and versus Er^{3+} concentration (for 45 W of pump power), respectively. The excitation densities are generally larger in the singly-doped system [open symbols in Figs. 3(b) and 4(b)]. Especially, the excitation density of the lower laser level is significantly smaller in the co-doped (solid squares) compared to the singly-doped system (open squares), because ET_1 to Pr^{3+} [circles with solid lines in Figs. 3(d) and 4(d)] depletes the lower laser level effectively. As a consequence, the population density of the upper laser level (solid triangles) is also smaller than in the singly-doped system (open triangles), because it is clamped to laser threshold.

Nevertheless, in the co-doped system, the excitation densities increase significantly with pump power [solid symbols in Fig. 3(b)], because lifetime quenching by ET_1 is not complete. Consequently, ETU from the laser levels becomes relevant at high pump powers [diamonds in Fig. 3(d)] and the slope efficiency can increase to values close to or even slightly higher than the Stokes limit of 35% in the co-doped fiber [Fig. 4(a), solid symbols]. An increase in the Pr^{3+} concentration would lead to a higher ET_1 rate, lower excitation densities, and a smaller influence from ETU, thereby further diminishing the energy-recycling effect and decreasing the slope efficiency. This dependence of the slope efficiency on Pr^{3+} concentration demonstrates the advantage of the energy-recycling regime in the singly-doped system at the Er^{3+} concentrations and pump powers investigated here.

At Er^{3+} concentrations above 5 mol.%, the population density of the lower laser level decreases with increasing Er^{3+}

concentration [squares in Fig. 4(b)]. This behavior reflects the corresponding increase of the parameter of ETU_1 (squares in Fig. 2) and, thus, the increasingly efficient depletion of the lower laser level by ETU_1. The effect is stronger in the singly- compared to the co-doped system, because the population density of the lower laser level is comparatively higher. Clearly, only Er^{3+} concentrations larger than approximately 5 mol.% can result in efficient energy recycling.

5) Relevant Loss Processes From the Upper Laser Level: Of the four possible loss processes from the upper laser level, namely intrinsic decay (fluorescence and multiphonon relaxation), ET, ESA, and ETU, the first two influence the laser threshold only but not the slope efficiency (Section IV-A). Furthermore, ET_2 to the Pr^{3+} co-dopant [circles with dotted lines in Figs. 3(d) and 4(d)] is inefficient because of the small oscillator strength of the corresponding absorption transition in Pr^{3+} [28]. The third process, ESA [triangles with dotted lines in Figs. 3(c) and (d), and 4(c) and (d)] is inefficient because of the relatively small amount of ground-state bleaching and excitation of the upper laser level in which this absorption process originates (Section IV-B-1).

ETU_2 from the upper laser level, however, plays an important role in the population mechanisms of the investigated systems. Although its parameter W_{22} is smaller than the parameter W_{11} of ETU from the lower laser level (Fig. 2), the population density of the upper laser level is higher than that of the lower laser level in many of the situations investigated [Figs. 3(b) and 4(b)]. This situation can lead to a higher rate of the former process. In the co-doped system, the lower laser level is quenched by ET to Pr^{3+}. Since the threshold inversion that is a linear function of the population densities of upper and lower laser levels must be maintained, the ratio of these population densities increases with increasing quenching of the lower laser level. In such a situation, ETU_2 (diamonds with dotted lines) from the upper exceeds ETU_1 (diamonds with solid lines) from the lower laser level at high Er^{3+} concentrations [Fig. 4(d)] for all pump powers [Fig. 3(d)]. The increased detrimental effect of ETU_2 from the upper laser level at the lower excitation densities present in the co-doped system is yet another reason why the lifetime-quenching regime will probably be inferior to the energy-recycling regime at the higher Er^{3+} concentrations at which ETU becomes the dominant depletion mechanism of both laser levels.

C. Optimization Criterion for the Energy-Recycling Regime

Only if ETU from the lower laser level has a significantly larger rate than both, the intrinsic decay from the same level and ETU from the upper laser level, the energy-recycling regime can produce slope efficiencies in excess of the Stokes efficiency and, thus, be advantageous over the lifetime-quenching regime [7]. From Fig. 2, we can see that the parameters of ETU from the laser levels increase with increasing Er^{3+} concentration because of the influence of energy migration [28]. However, the dependence on Er^{3+} concentration is different for the two ETU parameters, resulting in a rather complicated ratio of the two parameters (dashed line in Fig. 2). If intrinsic decay is negligible, the largest ratio of lower-to-upper-level ETU parameters provides the highest slope efficiency [17], [7]. The largest ratio is found for low Er^{3+} concentration, whereas this ratio is relatively constant at higher Er^{3+} concentrations.

For the higher Er^{3+} concentrations investigated, we find that the energy-transfer processes are, indeed, significantly more efficient than the intrinsic decay mechanisms of the laser levels. The intrinsic decay rates are, therefore, not shown in Figs. 3(c) and (d) or 4(c) and (d). At low Er^{3+} concentrations, however, the ETU processes become less efficient and intrinsic decay starts to play a role in the energy-recycling regime. The significant increase in slope efficiency with increasing Er^{3+} concentration in the energy-recycling regime [open symbols in Fig. 4(a)] to levels well in excess of the Stokes efficiency of 35% is, therefore, not a consequence of an optimized ratio of the ETU parameters, which would be obtained at lower Er^{3+} concentrations (Fig. 2), but merely a result of the successful competition of ETU_1 over intrinsic decay from the lower laser level.

This result for ZBLAN is in strong contrast to the behavior of the $LiYF_4:Er^{3+}$ laser. The latter system exhibits first, a smaller value of the macroscopic parameter of ETU_1 and, hence, reduced energy recycling from the lower laser level and second, a less favorable ratio of the ETU parameters. The maximization of the ETU ratio is, therefore, the major design criterion in the optimization of its laser performance [18], [32].

At the higher levels of Er^{3+} concentration (5–10 mol.%) investigated in our simulation, we expect that the slope efficiency obtained experimentally will not vary significantly with Er^{3+} concentration but will rather be influenced by the absorbed pump-power density in the fiber [open symbols in Fig. 4(a)]. From this point of view, it was important to optimize the fiber parameters relating to both, efficient pump coupling and absorption (Section III).

V. Conclusion

On the basis of our recent spectroscopic measurements of energy-transfer parameters, we have compared the population mechanisms that are present in Er^{3+} singly-doped and Er^{3+}, Pr^{3+} co-doped 3-μm fiber lasers under high-power diode pumping at 980 nm. This comparison was carried out as a function of pump power and Er^{3+} concentrations up to Er^{3+} concentrations that have recently become commercially available in ZBLAN fibers. It has been shown that the energy-recycling regime with its inherent enhancement of the slope efficiency by a factor of two can be exploited in highly Er^{3+}-doped ZBLAN fiber lasers. This approach will lead to superior performance compared to recent experimental demonstrations of high-power 3-μm fiber lasers that have used the co-doped system. For an incident pump power of 45 W available at 980 nm, the predicted optimum Er^{3+} concentration approaches 10 mol.%. Thermal problems that might possibly arise from the increased pump absorption could not be calculated and have to be checked experimentally. We expect output powers on the order of 10 W to become experimentally available in the near future, which would increase the output powers by almost an order of magnitude from currently available Er^{3+} 3-μm CW lasers. For future applications of this laser in micro-surgery, CW output powers of greater than 3 W would be required.

REFERENCES

[1] M. Frenz, H. Pratisto, F. Könz, E. D. Jansen, A. J. Welch, and H. P. Weber, "Comparison of the effects of absorption coefficient and pulse duration of 2.12 μm and 2.79 μm radiation on laser ablation of tissue," *IEEE J. Quantum Electron*, vol. 32, pp. 2025–2036, Dec. 1996.

[2] M. Krause, D. Steeb, H. J. Foth, J. Weindler, and K. W. Ruprecht, "Ablation of vitreous tissue with erbium : YAG laser," *Invest. Ophtalmol. Vis. Sci.*, vol. 40, no. 6, pp. 1025–1032, 1999.

[3] M. P. Goldman, N. Marchell, and R. E. Fitzpatrick, "Laser skin resurfacing of the face with a combined CO_2/Er : YAG laser," *Dermatol. Surg.*, vol. 26, no. 2, pp. 102–104, 2000.

[4] T. Wesendahl, P. Janknecht, B. Ott, and M. Frenz, "Erbium: YAG laser ablation of retinal tissue under perfluorodecaline: Determination of laser-tissue interaction in pig eyes," *Invest. Ophtalmol. Vis. Sci.*, vol. 41, no. 2, pp. 505–512, 2000.

[5] S. D. Jackson, T. A. King, and M. Pollnau, "Diode-pumped 1.7-W erbium 3-μm fiber laser," *Opt. Lett.*, vol. 24, no. 16, pp. 1133–1135, 1999.

[6] A. Y. Dergachev, J. H. Flint, and P. F. Moulton, "1.8-W CW Er: YLF diode-pumped laser," *Conf. Lasers and Electro-Optics—OSA Tech. Dig.*, p. 564, 2000.

[7] M. Pollnau and S. D. Jackson, "Erbium 3-μm fiber lasers," *IEEE J. Select. Topics Quantum Electron.*, vol. 7, pp. 30–40, Jan./Feb. 2001.

[8] M. Pollnau, E. Heumann, and G. Huber, "Time-resolved spectra of excited-state absorption in Er^{3+} doped $YAlO_3$," *Appl. Phys. A*, vol. 54, pp. 404–410, 1992.

[9] M. Pollnau, Ch. Ghisler, W. Lüthy, and H. P. Weber, "Cross-sections of excited-state absorption at 800 nm in erbium-doped ZBLAN fiber," *Appl. Phys. B*, vol. 67, no. 1, pp. 23–28, 1998.

[10] M. Pollnau, Ch. Ghisler, G. Bunea, M. Bunea, W. Lüthy, and H. P. Weber, "150 mW unsaturated output power at 3 μm from a single-mode-fiber erbium cascade laser," *Appl. Phys. Lett.*, vol. 66, no. 26, pp. 3564–3566, 1995.

[11] M. Pollnau, Ch. Ghisler, W. Lüthy, H. P. Weber, J. Schneider, and U. B. Unrau, "Three-transition cascade erbium laser at 1.7, 2.7, and 1.6 μm," *Opt. Lett.*, vol. 22, no. 9, pp. 612–614, 1997.

[12] L. Wetenkamp, "Charakterisierung von laseraktiv dotierten Schwermetallfluorid-Gläsern und Faserlasern," Ph.D. dissertation, Institute of High-Frequency Technique, Technical University of Braunschweig, Braunschweig, Germany, 1991.

[13] D. S. Knowles and H. P. Jenssen, "Upconversion versus Pr-deactivation for efficient 3 μm laser operation in Er," *IEEE J. Quantum Electron.*, vol. 28, pp. 1197–1208, Apr. 1992.

[14] M. Pollnau, "The route toward a diode-pumped 1-W erbium 3-μm fiber laser," *IEEE J. Quantum Electron.*, vol. 33, pp. 1982–1990, Nov. 1997.

[15] S. D. Jackson, T. A. King, and M. Pollnau, "Efficient high power operation of erbium 3 μm fiber laser diode-pumped at 975 nm," *Electron. Lett.*, vol. 36, no. 3, pp. 223–224, 2000.

[16] K. S. Bagdasarov, V. I. Zhekov, V. A. Lobachev, T. M. Murina, and A. M. Prokhorov, "Steady-state emission from a $Y_3Al_5O_{12} : Er^{3+}$ laser ($\lambda = 2.94\ \mu,\ T = 300\ ^\circ$K)," *Kvant. Elektr.*, vol. 10, pp. 452–454, 1983.

[17] M. Pollnau, R. Spring, Ch. Ghisler, S. Wittwer, W. Lüthy, and H. P. Weber, "Efficiency of erbium 3-μm crystal and fiber lasers," *IEEE J. Quantum Electron.*, vol. 32, pp. 657–663, Apr. 1996.

[18] T. Jensen, A. Diening, G. Huber, and B. H. T. Chai, "Investigation of diode-pumped 2.8-μm Er : $LiYF_4$ lasers with various doping levels," *Opt. Lett.*, vol. 21, no. 8, pp. 585–587, 1996.

[19] Ch. Wyss, W. Lüthy, H. P. Weber, P. Rogin, and J. Hulliger, "Emission properties of an optimized 2.8 μm Er^{3+} : YLF laser," *Opt. Commun.*, vol. 139, no. 4–6, pp. 215–218, 1997.

[20] D.-W. Chen, C. L. Fincher, T. S. Rose, F. L. Vernon, and R. A. Fields, "Diode-pumped 1-W continuous-wave Er : YAG 3-μm laser," *Opt. Lett.*, vol. 24, no. 6, pp. 385–387, 1999.

[21] T. Sandrock, D. Fischer, P. Glas, M. Leitner, M. Wrage, and A. Diening, "Diode-pumped 1-W Er-doped fluoride glass M-profile fiber laser emitting at 2.8 μm"," *Opt. Lett.*, vol. 24, no. 18, pp. 1284–1286, 1999.

[22] B. Srinivasan, E. Poppe, J. Tafoya, and R. K. Jain, "High-power (400 mW) diode-pumped 2.7 μm Er : ZBLAN fibre lasers using enhanced Er–Er cross-relaxation processes," *Electron. Lett.*, vol. 35, no. 16, pp. 1338–1340, 1999.

[23] S. C. Tidwell, J. F. Seamans, M. S. Bowers, and A. K. Cousins, "Scaling CW diode-end-pumped Nd : YAG lasers to high average powers," *IEEE J. Quantum Electron.*, vol. 28, pp. 997–1009, Apr. 1992.

[24] A. K. Cousins, "Temperature and thermal stress scaling in finite-length end-pumped laser rods," *IEEE J. Quantum Electron.*, vol. 28, pp. 1057–1069, Apr. 1992.

[25] C. Pfistner, R. Weber, H. P. Weber, S. Merazzi, and R. Gruber, "Thermal beam distortions in end-pumped Nd : YAG, Nd : GSGG, and Nd : YLF rods," *IEEE J. Quantum Electron.*, vol. 30, pp. 1605–1615, July 1994.

[26] M. Pollnau, P. J. Hardman, M. A. Kern, W. A. Clarkson, and D. C. Hanna, "Upconversion-induced heat generation and thermal lensing in Nd : YLF and Nd : YAG," *Phys. Rev. B*, vol. 58, no. 24, pp. 16 076–16 092, 1998.

[27] M. Pollnau, "Heat generation and thermal lensing in 2.8-μm Er^{3+} : $LiYF_4$ lasers," in *Conf. Lasers and Electro-Optics Pacific Rim, 1999 Tech. Dig.*, 1999, pp. 738–739.

[28] P. S. Golding, S. D. Jackson, T. A. King, and M. Pollnau, "Energy-transfer processes in Er^{3+}-doped and Er^{3+}, Pr^{3+}-codoped ZBLAN glasses," *Phys. Rev. B*, vol. 62, no. 2, pp. 856–864, 2000.

[29] R. S. Quimby, W. J. Miniscalco, and B. Thompson, "Excited state absorption at 980 nm in erbium doped glass," in *Fiber Laser Sources and Amplifiers III*: SPIE, 1991, vol. 1581, pp. 72–79.

[30] V. K. Bogdanov, W. E. K. Gibbs, D. J. Booth, J. S. Javorniczky, P. J. Newman, and D. R. MacFarlane, "Fluorescence from highly-doped erbium fluorozirconate glasses pumped at 800 nm," *Opt. Commun.*, vol. 132, no. 1–2, pp. 73–76, 1996.

[31] S. D. Jackson, T. A. King, and M. Pollnau, "Modelling of high-power diode-pumped erbium 3-μm fibre lasers," *J. Modern Opt.*, vol. 47, no. 11, pp. 1987–1994, 2000.

[32] T. Jensen, "Upconversion-Prozesse und Wirkungsquerschnitte in Er^{3+}-dotierten 3 μm Fluorid- und Granat-Lasern, gepumpt mit cw und quasicw Dioden-Arrays," Ph.D. dissertation, Institute of Laser-Physics, University of Hamburg, Hamburg, Germany, 1996.

[33] K. S. Bagdasarov, V. I. Zhekov, V. A. Lobachev, T. M. Murina, and A. M. Prokhorov, "Steady-state emission from a $Y_3Al_5O_{12} : Er^{3+}$ laser ($\lambda = 2.94\ \mu,\ T = 300\ ^\circ$K)," *Sov. J. Quantum Electron.*, vol. 13, no. 2, pp. 262–263, 1983.

Markus Pollnau received the Diploma in physics from the University of Hamburg, Hamburg, Germany, in 1992, and the Ph.D. degree in physics from the University of Bern, Bern, Switzerland, in 1996.

From 1996 to 1998, he was with the University of Southampton, Southampton, U.K., as Research Fellow of the European Union, and from 1998 to 1999, at the University of Bern. From 1998 to 2000, he was also a Visiting Researcher at the University of Manchester, Manchester, U.K. In 1999, he joined the Institute of Applied Optics at the Swiss Federal Institute of Technology, Lausanne, as a "Profil" fellow of the Swiss National Science Foundation. His current research interests are in the fields of broadband light sources based on transition-metal-ion and rare-earth-ion doped waveguide structures for applications in optical coherence tomography and high-power fiber lasers for applications in micro-surgery. He has co-authored over 70 technical contributions in international journals and conferences.

Dr. Pollnau is a member of the European, German, and Swiss Physical Societies and the Optical Society of America.

Stuart D. Jackson received the B.Sc. degree in 1989 and the B.Sc. (Hons.) degree in 1990, both from the University of Newcastle, Newcastle, Australia, and the Ph.D. degree from the Centre for Lasers and Applications, Macquarie University, Macquarie, Australia, in 1996.

In 1995, he joined the Laser Photonics Group at the University of Manchester, Manchester, U.K., and carried out post-doctoral research into high-power fiber lasers. In 1999, he joined the Optical Fiber Technology Centre, University of Sydney, Sydney, Australia, where he is now an Australian Research Fellow, sponsored by the Australian Research Council.